

# Spectral detection of multiple stellar populations in $z \sim 1$ early-type galaxies

I. Lonoce,<sup>1,2\*</sup> M. Longhetti,<sup>1</sup> P. Saracco,<sup>1</sup> A. Gargiulo,<sup>1</sup> S. Tamburri<sup>1,2</sup>

<sup>1</sup>*INAF-Osservatorio Astronomico di Brera, via Brera 28, 20121 Milano, Italy*

<sup>2</sup>*Dipartimento di Scienza e Alta Tecnologia, Università degli Studi dell'Insubria, via Valleggio 11, 22100 Como, Italy*

Accepted 2014 August 5. Received 2014 July 4; in original form 2014 January 24

## ABSTRACT

We present a spectroscopic analysis based on measurements of two mainly age-dependent spectrophotometric indices in the 4000Å rest frame region, i.e. H+K(CaII) and  $\Delta 4000$ , for a sample of 15 early-type galaxies (ETGs) at  $0.7 < z_{spec} < 1.1$ , morphologically selected in the GOODS-South field. Ages derived from the two different indices by means of the comparison with stellar population synthesis models, are not consistent with each other for at least nine galaxies (60 per cent of the sample), while for the remaining six galaxies, the ages derived from their global spectral energy distribution (SED) fitting are not consistent with those derived from the two indices. We then hypothesized that the stellar content of many galaxies is made of two stellar components with different ages. The double-component analysis, performed by taking into account both the index values and the observed SED, fully explains the observational data and improves the results of the standard one-component SED fitting in 9 out of the 15 objects, i.e. those for which the two indices point towards two different ages. In all of them, the bulk of the mass belongs to rather evolved stars, while a small mass fraction is many Gyr younger. In some cases, thanks to the sensitivity of the H+K(CaII) index, we find that the minor younger component reveals signs of recent star formation. The distribution of the ages of the younger stellar components appears uniformly in time and this suggests that small amounts of star formation could be common during the evolution of high- $z$  ETGs. We argue the possibility that these new star formation episodes could be frequently triggered by internal causes due to the presence of small gas reservoir.

**Key words:** galaxies: elliptical and lenticular, cD – galaxies: evolution – galaxies: formation – galaxies: high-redshift – galaxies: stellar content.

## 1 INTRODUCTION

Early-type galaxies (elliptical and lenticular, hereafter ETGs) are well-known precious high-redshift candidates to trace observationally the formation and evolution of the main structures in the Universe, since they are the most massive and so the brightest galaxies and contain most of the local observed stars and baryons (Renzini 2006 and references therein). Also the homogeneous properties of their stellar content put them in a privileged position to explore the history of their stellar mass assembly.

Despite the lower quality and quantity of high-redshift data, direct measurements on the stellar populations of high- $z$  galaxies still remain the best solid way to constrain the earlier evolution of ETGs (Van der Wel et al. 2005; Cappellari et al. 2009; Guo et al. 2011; Strazzullo et al.

2013). In fact, the possibility of detecting direct pieces of evidence of stellar evolution, both through photometric and spectroscopic data, is almost unique in a redshift range, i.e.  $1 < z < 2$ , where most of the ETG evolution is expected (Cimatti et al. 2004; Glazebrook et al. 2004). A second convenience of dealing with high- $z$  data is the more reliable use of the synthetic modelling which, thanks to the relative young ages of high- $z$  sources, is significantly less affected by degeneracy effects, e.g. age-metallicity degeneracy which is dominant in the local ETGs.

Up to now, the most used method to explore the stellar population properties of high- $z$  ETGs is the analysis of the spectral energy distribution (SED) by means of multi-band photometry (Daddi et al. 2005; Longhetti & Saracco 2009; Santini et al. 2009; Sanchez et al. 2011). However, the physical parameters extracted from the SED fitting process on synthetic models, like in particular age, are actually only indicative mean values; thus, this method misses the detec-

\* E-mail: [ilaria.lonoce@brera.inaf.it](mailto:ilaria.lonoce@brera.inaf.it) (OAB)

tion of the possible presence of inhomogeneities in the stellar content. In contrast, a restricted but more detailed spectroscopic analysis would be an interesting challenge to unveil that information lost in the whole SED analysis.

The important goal to be reached through the analysis of the stellar population properties of galaxies observed at  $z \sim 1$  in their critical state of evolution, is to understand if all of their stars are coeval and still passively evolving, as they are usually modelled with  $z_{form} > 2-3$  (Renzini 2006), or there are some pieces of evidence of later star forming episodes or minor merging events which led to composite stellar populations already at  $z \sim 1$ .

The hidden complexity of the star formation history of ETGs has been revealed by many works on local ETGs (Coccatto et al. 2010; Panuzzo et al. 2011; Kaviraj et al. 2012; Rocca-Volmerange et al. 2013), and at intermediate redshift (Treu et al. 2002), where different kinds of signature suggest that elliptical galaxies have possibly undergone rejuvenation episodes in their recent history. Also at high redshift, with both archaeological and direct measurements, the necessity of introducing multiple stellar populations, with different stellar properties, in the used modelling has been found (Gargiulo et al. 2012; Huang et al. 2013). The main stellar properties involved in the differentiation of stellar components are age and metallicity. However, age is surely the first stellar parameter which should be investigated on high- $z$  ETGs. In fact, direct spectroscopic measurements of stellar metallicity on high- $z$  ETGs are still a hard issue; moreover, Gargiulo et al. (2012) found that age gradients are necessary to reproduce the majority of the observed high- $z$  colour gradients.

Coexistent different stellar populations in ETGs are expected from the theoretical models on galaxy formation and evolution: minor mergers and small accretion events instead of major mergers, in fact, are predicted to be frequent until  $z = 0$  (Naab et al. 2009; Oser et al. 2010, 2012). This inside out formation scenario, however, predicts that for high mass galaxies, accreted stars have been formed in the same epoch of “*in situ*” stars (Oser et al. 2010), assembling thus composite stellar populations of rather coeval stellar content, though the minor mergers have occurred at different times.

So the attention now should be focused on finding some observables which allow one to understand how homogeneous are the stellar populations of elliptical galaxies and how important are the mass fraction and the age of the accreted stars. A spectroscopic analysis on a sample of high- $z$  ETGs can surely reveal precious details on their stellar properties, to shed light on the composition of the stellar populations of galaxies in their earlier phases of evolution. Previously, other pioneer works (Onodera et al. 2012; Jørgensen & Chiboucas 2013) have been devoted to the analysis of spectroscopic high- $z$  data, revealing many differences in the stellar properties of  $z > 1$  objects with respect to local ETGs, such as the presence of extreme values of spectral indices not foreseen by models (Onodera et al. 2012). In this paper we present our spectroscopic analysis of a small sample of ETGs based on some of the first high quality optical spectroscopic data at  $z \sim 1$  in the GOODS-South field, which, thanks to the measurements of reliable age-dependent spectrophotometric indices in the 4000Å rest frame region, i.e. the H+K(CaII) and  $\Delta 4000$ , has led to interesting results on this topic.

The paper is organized as follows: in Section 2 we introduce our sample and describe the spectroscopic data with the main passes of the data reduction. In Section 3 we present the definition and the measurements of the spectrophotometric indices which are the basis of our spectral analysis. The comparison of the obtained results with synthetic stellar population models is widely discussed in Section 4, together with the description of our proposed double-component models. In Section 5 we discuss our results through the comparison with other works based on high- $z$  spectral analysis. We propose the summary and our conclusion in Section 6.

Throughout this paper, we assume a standard cosmology with  $H_0 = 70 \text{ km s}^{-1} \text{ Mpc}^{-1}$ ,  $\Omega_m = 0.3$  and  $\Omega_\Lambda = 0.7$ . All photometric magnitudes are expressed in the AB system.

## 2 THE SAMPLE

The sample consists of 15 ETGs at  $0.7 < z_{spec} < 1.1$  morphologically selected from a catalogue complete to  $K \simeq 22$  (Tamburri et al., in preparation), in the southern field of the Great Observatories Origins Deep Survey (GOODS-South v2; Giavalisco et al 2004). The selection criterion of this sample was basically the availability of sufficient high-quality ( $S/N > 5$ ) spectroscopic data to perform the measurements of the main spectrophotometric indices in the 4000Å break region, which is the aim of this work. Thus, starting from the complete sample of 196 morphologically selected ETGs with  $K < 22$ , only 15 could provide a high-S/N spectrum suitable for the present study (see Section 2.1 for details).

All the selected galaxies have the 14 bands GOODS-South survey coverage (Santini et al. 2009): deep optical images taken from four *Hubble Space Telescope*-Advance Camera for Surveys bandpasses ( $F435W$ ,  $F606W$ ,  $F775W$  and  $F850LP$ ); photometric data provided by extensive observations of European Southern Observatory (ESO) telescopes both in the optical (three  $U$ -band filters) and in the near-infrared ( $J$ ,  $H$  and  $K$  filters), and by the four *Spitzer-Infrared Array Camera* bands (3.6, 4.5, 5.8 and  $8.0\mu\text{m}$ ).

Thanks to these multiwavelength data we were able to perform the global SED fitting of all the galaxies of the sample in order to extract the global stellar population properties. The SED fitting process was carried out assuming the stellar population synthesis model of Bruzual and Charlot (Bruzual & Charlot 2003) (hereafter BC03) with a Chabrier initial mass function (IMF)(Chabrier 2003). We adopted star formation histories with five exponentially declining star formation rates with  $e$ -folding time  $\tau = [0.1, 0.3, 0.4, 0.6, 1.0]$  Gyr and assumed solar metallicity  $Z = 0.020$ . Dust extinction, following Calzetti et al. (2000), was applied in the range  $0 < A_v < 2$  mag. In Table 1, we report the stellar parameters obtained from the SED fitting of the 15 ETGs: photometric ages  $Age_{phot}$  of the stellar populations, dust extinction  $A_v$ , stellar masses  $\mathcal{M}_*$  and star formation time-scale  $\tau$ .

For five objects out of the whole sample (those at the highest spectral resolution) the velocity dispersion measures are available (Van der Wel et al. 2005). Furthermore, 7 out of the 15 target galaxies (those at  $z > 0.9$ ) are included in the complete sample of the GOODS-South field ETGs at  $z > 0.9$  (Saracco et al. 2010).

**Table 1.** Sample of 15 ETGs. Data extracted from photometric analysis: stellar population age ( $A_{phot}$ ), dust extinction ( $A_v$ ), logarithm of the stellar mass ( $\log(\mathcal{M}_*)$ ) and star formation time-scale ( $\tau$ ).  $\sigma$  is the velocity dispersion measured by Van der Wel et al. (2005). Units of right ascension are hour, minutes and seconds, and units of declination are degrees, arcminutes and arcseconds.

ID-MUSIC	RA	Dec	$z_{spec}$	Age <sub>phot</sub> (Gyr)	$A_v$ (mag)	$\log(\mathcal{M}_*)$ ( $M_\odot$ )	$\tau$ (Gyr)	$\sigma$ ( $\text{km s}^{-1}$ )
1192 <sup>a</sup>	3:32:25.16	-27:54:50.1	1.089	0.7	1.0	11.01	0.1	231±15
1382 <sup>a</sup>	3:32:22.93	-27:54:34.3	0.964	1.4	0.4	11.08	0.1	200±9
1950 <sup>a</sup>	3:32:26.29	-27:54:05.0	1.044	1.9	0.3	10.75	0.3	300±30
1837 <sup>a</sup>	3:32:19.29	-27:54:06.1	0.964	3.0	0.4	11.40	0.4	336±18
2694 <sup>a</sup>	3:32:31.37	-27:53:19.1	1.135	2.5	0.3	11.40	0.3	232±19
9066 <sup>a</sup>	3:32:33.06	-27:48:07.5	1.188	2.0	0.6	10.58	0.3	-
11539 <sup>a</sup>	3:32:37.19	-27:46:08.1	1.096	2.3	0.5	11.42	0.3	-
10020	3:32:15.81	-27:47:13.6	0.738	1.8	0.5	10.85	0.3	-
10960	3:32:19.24	-27:46:32.2	0.737	2.4	0.3	10.76	0.3	-
11225	3:32:14.44	-27:46:24.5	0.736	1.4	0.2	10.22	0.1	-
9792	3:32:18.01	-27:47:18.6	0.734	3.25	0.5	11.58	0.4	-
13386	3:32:17.49	-27:44:36.7	0.734	1.7	0.3	10.31	0.3	-
9838	3:32:17.94	-27:47:21.5	0.732	3.25	0.2	11.08	0.4	-
17044	3:32:37.38	-27:41:26.2	0.672	3.25	0.1	11.21	0.4	-
7424	3:32:39.54	-27:49:28.4	0.669	2.6	0.2	10.54	0.4	-

<sup>a</sup>objects belonging to 34 ETGs of Saracco et al. (2010).

## 2.1 Spectroscopic data

As already mentioned, our sample of ETGs was collected following the disponibility of high-S/N optical spectra in the GOODS-South field for galaxies morphologically confirmed as ETGs with  $z \sim 1$ . High-quality spectra come from three different observing campaigns: one summarized in Mignoli et al. (2005) (K20 survey), one in Popesso et al. (2009) and in Van der Wel et al. (2005). We could not use spectra coming from the campaign VLT/FORS2 spectroscopy in the GOODS-South field reported in Vanzella et al. (2005, 2008), because observations have been made without the cut order filter OG590+32, so they have not a solid continuum shape calibration necessary for the measurement in particular of the  $\Delta 4000$  index.

The K20 survey is a near-infrared-selected redshift survey targeting galaxies ( $K_s < 20$ , Vega system) in two fields, one of which has been later included in the GOODS-South area. From this precious data base of public galaxy spectra (<http://vizier.u-strasbg.fr/viz-bin/VizieR?-source=J/A%2BA/432/0853>), we have searched for the highest S/N spectra of  $z \geq 0.7$  ETGs in the  $4000\text{\AA}$  break region rest frame. We finally extracted eight ETGs in the redshift range  $0.73 < z < 1.2$ . Spectroscopic observations of these objects come from VLT-FORS1 in MOS mode and VLT-FORS2 in MXU mode (multi-object spectroscopy with exchangeable masks), with a set of grisms 150I, 200I and 300I providing dispersion of 5.5, 3.9 and 2.6  $\text{\AA}/\text{pixel}$  and spectral resolution of  $R = 260$ , 380 and 660 respectively. The observation period of the K20 spectroscopic survey was confined in 20 nights during four years (1999-2000, 2002). For more details, see Mignoli et al. (2005).

Our next source of optical spectra was the second campaign of the ESO-GOODS spectroscopic programme operated with VLT-VIMOS (Visible MultiObject Spectrograph) and reported in Popesso et al. (2009). From the thousands of available spectra we have looked for the ones with longer exposure time (exp-time  $> 5\text{h}$ ) in order to reach the highest

S/N for  $z > 0.7$  ETGs. Moreover, our searching has been focused only on median resolution (MR - resolution  $R = 580$ , dispersion  $2.5\text{\AA}/\text{pixel}$ ) grism data, necessary to perform the measurements of the spectrophotometric indices. We found only 2 suitable objects in the redshift range  $z \sim 0.7-1.0$ . Observations were carried on during the winter of 2004-2005 for both objects. For deeper details, see Popesso et al. (2009).

Finally, the last five objects of our sample were analysed by means of the optical spectra coming from observations performed by Van der Wel et al. (2005) with FORS2 in MXU mode on VLT telescope. They used the GRIS-600z grism together with the OG590 order separation filter, with a resolution of  $R \sim 1390$ , that led to a binned spectral dispersion of  $1.6\text{\AA}/\text{pixel}$  and a wavelength coverage from about  $6500$  to  $11000\text{\AA}$  (that means around the spectral region of the Balmer/ $4000\text{\AA}$  break for galaxies at  $z \sim 1$ ). The observations of the five objects were carried out in the period from 2002 September to 2003 March, with a mean exposure time of about 11 h for object (for details, see Van der Wel et al.

All the details of the spectroscopic data are summarized in Table 2.

## 2.2 Data reduction

Spectra coming from Popesso et al. (2009) and Van der Wel et al. (2005) have been reduced starting from raw observed data. For K20-survey spectra, we used directly the online material (from Vizier: “K20 survey: spectroscopic catalogue (Mignoli et al. 2005)”). Standard spectral data reduction has been applied using IRAF software tools. Particular care has been devoted to the relative spectral flux calibration, which has been achieved using spectrophotometric standard stars observed in the same nights of the targets; in particular, for VLT-FORS2 data (Van der Wel et al. 2005), we took the mean sensitivity function built with standard stars of different spectral type, which reveal small intrinsic differences in their shape.

**Table 2.** Information about the spectroscopic data used in this work: spectroscopic instrument, grism, dispersion, resolution and the observing run.

ID-MUSIC	Instrument	Grism	Dispersion (Å/pixel)	Resolution	Observing run
1192	VLT-FORS2	600z	1.6	1390	Van der Wel et al. (2005)
1382	VLT-FORS2	600z	1.6	1390	Van der Wel et al. (2005)
1950	VLT-FORS2	600z	1.6	1390	Van der Wel et al. (2005)
1837	VLT-FORS2	600z	1.6	1390	Van der Wel et al. (2005)
2694	VLT-FORS2	600z	1.6	1390	Van der Wel et al. (2005)
9066	VLT-FORS2	300I	2.6	660	Mignoli et al. (2005)
11539	VLT-FORS2	200I	3.9	380	Mignoli et al. (2005)
10020	VLT-FORS1	150I	5.5	260	Mignoli et al. (2005)
10960	VLT-FORS2	150I	5.5	260	Mignoli et al. (2005)
11225	VLT-FORS2	200I	3.9	380	Mignoli et al. (2005)
9792	VLT-FORS1	150I	5.5	260	Mignoli et al. (2005)
13386	VLT-FORS2	200I	3.9	380	Mignoli et al. (2005)
9838	VLT-FORS1	150I	5.5	260	Mignoli et al. (2005)
17044	VLT-VIMOS	MR	2.5	580	Popesso et al. (2009)
7424	VLT-VIMOS	MR	2.5	580	Popesso et al. (2009)

Moreover, still with the aim of obtaining the best continuum shape calibration necessary for a solid measure of spectral indices, we applied a further continuum calibration on the VLT-FORS2 spectra: indeed we noted a systematic distortion of the spectrum shape for objects whose slits are shifted with respect to the central position, along the dispersion direction (see details in Longhetti et al., in preparation). The amount of the flux distortion is proportional to the distance of the slit from the central position and, in the particular case of our VLT-FORS2 objects, the maximum offset slit position leads to a variation up to about 30 per cent of the flux. We corrected for this further distortion using flat-field lamp spectra as standard spectral sources, available for all the slits. The ratio between the wavelength-calibrated flat-field spectrum obtained in a central position and the one obtained through each slit in offset position has been used for this further correction. The final check of the obtained continuum shape accuracy in the spectral region involved in the measure of the chosen spectrophotometric indices, was to overlap the final 1D spectra with the photometric points in the optical bands. The agreement is reached within 1- $\sigma$  error from the photometric points.

Reduced monodimensional spectra of the whole sample are shown in Figure 1 together with the principal absorption lines in the region of 4000Å rest frame.

### 3 SPECTRAL INDEX MEASURES

As can be seen in Figure 1, many absorption lines typical of the stellar atmospheres can be identified in the optical spectra of our selected sample: Balmer series, BL3580, CN, CaII(H,K), Gband. We have taken advantage of the quality of our sample spectra of ETGs in order to analyse the main properties of their stellar populations, in particular the *age* of their stellar content.

The most important age-dependent spectrophotometric indices in the observed optical region are: the  $\Delta 4000$  index, defined by Bruzual (1983) and Hamilton (1985) as the ratio between mean fluxes in two different wide spectral ranges

around the 4000Å rest frame

$$\Delta 4000 = \frac{\bar{F}_\nu(\lambda_1 - \lambda_2)}{\bar{F}_\nu(\lambda_3 - \lambda_4)} \quad (1)$$

with  $\lambda_1 - \lambda_2 = [4050\text{Å} - 4250\text{Å}]$ ,  $\lambda_3 - \lambda_4 = [3750\text{Å} - 3950\text{Å}]$ ; and the H+K(CaII) index, defined by Rose (1985) as the ratio between minimum fluxes of the two CaII absorption lines H and K

$$H + K(\text{CaII}) = \frac{F_{\min}(\lambda_3, \lambda_4)}{F_{\min}(\lambda_1, \lambda_2)} \quad (2)$$

with  $\lambda_1 = 3926$ ,  $\lambda_2 = 3940$ ,  $\lambda_3 = 3961$ ,  $\lambda_4 = 3975$ . In particular, the CaII(H) absorption line is blended with the Balmer H $\epsilon$  at  $\lambda = 3969.65\text{Å}$  (see details in Longhetti et al. 1999).

The choice of measuring the values of these two spectrophotometric indices was supported by their intrinsic peculiarities. In fact, these indices not only are strongly dependent on stellar population's age variations, mainly for ages less than 6-7 Gyr which is about the age of Universe at  $z \sim 1$ , but they also present precious differences which have made their combined measure very interesting.

The  $\Delta 4000$  index provides a measure of the age of the global stellar population: in fact, according with its definition, this index evaluates the ratio of the old and red stars flux with respect to the UV flux emission of the younger population. Higher is its value, older is the stellar content. The effect of the metallicity goes in the same direction of ageing, but this degeneracy is minimal for stellar populations younger than 6-7 Gyr (the upper limit of the age of our high- $z$  galaxies sample). On the other hand, the H+K(CaII) index is deeply dependent on the presence of young stellar populations: in fact, the ratio between H and K(CaII) lines would be constant if it was not for the blend of H(CaII) with Balmer H $\epsilon$ , which actually determines the index value. In particular, the effective ratio between H(CaII)+H $\epsilon$  and K(CaII) becomes  $< 1$  only for hot stars of type earlier than F5 which have strong Balmer series absorptions, with a minimum value for A-type Balmer-dominated stars (Rose 1985).

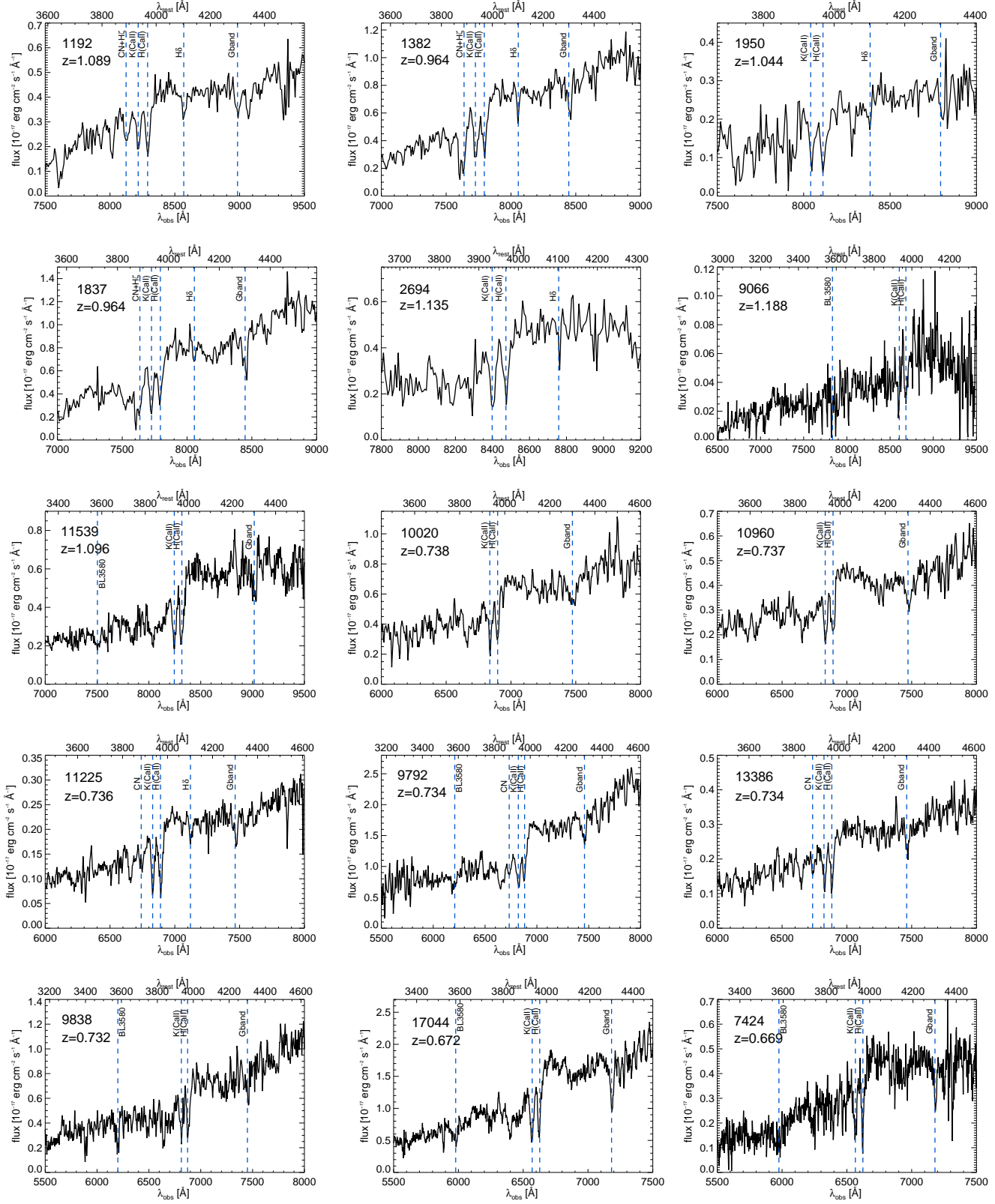


**Figure 1.** Spectra of the sample galaxies with the main absorption lines in the region of the Balmer/4000 $\text{\AA}$  break. Information about the spectroscopic data is shown in Table 2. Spectra are shown in bins spanning from 2.5 to 8  $\text{\AA}$ .

We measured  $\Delta 4000$  and H+K(CaII) indices on the spectra of our sample of ETGs, and results are reported in Table 3. It is worthy to note that the measure of the H+K(CaII) index is sensitive to the spectral resolution of the spectral data (see Longhetti et al. 1999), and we take this into account when comparing measures with models. Indeed, each measure performed on the spectra was corrected by the corresponding factor which brings the index value as it was measured on a spectrum with the higher resolution of models. In order to obtain these correction factors, we have degraded the spectrum of a reference template, with the original resolution full width at half-maximum (FWHM)= 3 Å (in the spectral range 3000 – 5000 Å rest frame), to the lower resolutions of the observed spectra. We derived the correction factors by dividing the index values measured on the degraded spectra by those measured on the reference template. In particular, these correction factors decrease the index values up to about 5 per cent of their measured values in the case of the lower resolution grism (R= 260).

Furthermore, the broadening of the absorption lines due to the intrinsic velocity dispersion of galaxies affects the measure of this index. We thus corrected the raw H+K(CaII) index measures obtained on the five ETGs observed at the highest spectral resolution (Van der Wel et al. 2005) for this effect, reporting them to the case of null velocity dispersion. We followed the same procedure as for the resolution correction: taking a reference template spectrum which has the same spectral resolution of Van der Wel et al. (2005) data, we enlarged their spectral lines convolving them with a Gaussian curve with different  $\sigma$  in order to simulate the effect of the velocity dispersion. We measured the H+K(CaII) index values for each value of the applied velocity dispersion and derived the correction factors to be applied to the index measurements. The correction factors were found to be rather small and well within the error bars. In particular, for three objects the correction was within 2 per cent of the measured value, and for the other two objects it was about 4 per cent. For all the other 10 ETGs of our sample, the lower spectral resolution of their observations prevents to appreciate the latter effect, being much larger than the broadening caused by the resolution itself. Indeed, we have verified that for the medium-resolution spectra (Popesso et al. 2009), the corresponding correction factors, assuming a typical velocity dispersion of 250 km/s, would be less than 1 per cent of the measured index values.

Errors have been computed from the uncertainties in the measures of fluxes and in the flux calibration. In particular, we have estimated the values of S/N ratios in the two spectral regions involved in the index definitions (i.e. 3750 – 4000Å and 4050 – 4250Å) which represent the statistical errors affecting the flux values. On the other hand, we took into account also the flux calibration uncertainties derived from both the standard flux calibration and from the further correction applied on the FORS-2 spectra which suffer for the shape distortion due to the CCD slit position (see Section 2.2). Obviously, the H+K(CaII) index, being the flux ratio at two very close wavelengths, is almost unaffected by these flux calibration uncertainties. The final errors are shown in Table 3.

**Table 3.** Values of the measured H+K(CaII) and  $\Delta 4000$  indices.

ID-MUSIC	H+K(CaII)	$\Delta 4000$
1192	0.75±0.07	1.80±0.04
1382	1.14±0.07	2.15±0.07
1950	0.97±0.23	2.05±0.1
1837	1.49±0.10	2.16±0.3
2694	1.07±0.16	1.87±0.06
9066	1.34±0.27	1.65±0.10
11539	1.15±0.11	2.10±0.05
10020	1.57±0.23	1.84±0.06
10960	1.31±0.20	1.72±0.04
11225	0.91±0.13	1.81±0.03
9792	1.15±0.13	2.09±0.04
13386	0.97±0.15	1.76±0.03
9838	0.84±0.20	1.99±0.06
17044	1.16±0.12	2.05±0.02
7424	0.58±0.23	1.81±0.07

#### 4 ANALYSIS

The measured values of the indices have been compared with the expectations of the spectro-photometric synthesis models (BC03) assuming a Chabrier IMF and an exponentially declining star formation history with time-scale  $\tau$  (with the same assumptions of the photometric analysis, see Section 2, i.e.  $\tau = 0.1 - 1$  Gyr and solar metallicity; afterwards we will discuss the effects of varying these assumptions). Indeed, to start with the simpler evolutionary modelling of star formation typical of ETGs, we assumed that the bulk of the star formation activity has happened in a confined initial episode with small time-scale  $\tau$  ( $\tau < 1$  Gyr, as it is the case of ETGs, see Saracco et al. (2010)). In this scenario, the stellar content of galaxies is rather coeval, within  $\tau$ , so if this evolutionary modelling is appropriate for the real star formation history of ETGs, we expected that the stellar ages derived from the values of the two indices would be consistent with each other.

Figure 2 shows the comparison between data and models in the  $\Delta 4000$  versus H+K(CaII) plane. Black dots are galaxies from the spectroscopic sample of Van der Wel et al. (2005), red ones from Mignoli et al. (2005) and blue ones from Popesso et al. (2009). Lines represent the trends of the values of the two indices of synthetic models at different ages, from younger ages ( $10^8$  yr) at the bottom left to older ages ( $10^{10}$  yr) at the upper right (at fixed solar metallicity), and their colours show different star formation histories determined by the time-scale parameter  $\tau$ . From Figure 2 it is possible to notice that: *i*) data points cover an extended area in the index index plane which corresponds to stellar populations older than  $\sim 2.5$  Gyr; *ii*) different  $\tau$ -models (coloured lines) are confined in a rather thin strip, while measured data are more widespread. While the majority of the data points are in agreement with models, we get the evidence that for 6 out of 15 objects both indices deviate at more than  $1\sigma$  from models. In particular, starting from the measured values of the  $\Delta 4000$  index, 7 out of 15 data points have: either too low values of the H+K(CaII) index (IDs: 1192, 7424 and 9838), suggesting possible stellar populations younger than what pointed out from the  $\Delta 4000$  index (see Section 3), or so high values of the H+K(CaII) index ( $H+K(CaII) > 1.2$ , IDs: 9066, 10960, 10020 and 1837) that they cannot find

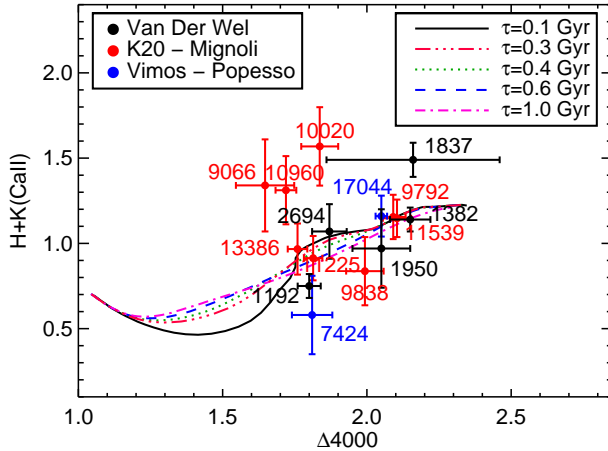


**Figure 2.** Data versus model comparison in the index index plane: measured values of the indices  $\Delta 4000$  ( $x$ -axis) and  $H+K(\text{CaII})$  ( $y$ -axis) from the spectroscopic sample of Van der Wel et al. (2005) (black dots), Mignoli et al. (2005) (red dots) and Popesso et al. (2009) (blue dots), compared with the expectations of BC03 models at different ages (from left to right, from about  $10^8$  to  $10^{10}$  yr), fixed solar metallicity and for different star formation time-scale parameters  $\tau$  (colored lines). With the exception of those from Van der Wel et al. (2005) sample, shown data points have  $H+K(\text{CaII})$  index values a bit underestimated (within error bars) with respect to those indicated by models due to the difference between the spectral resolutions of BC03 synthetic spectra ( $\text{FWHM} = 3\text{\AA}$ ) and that of the observed ones (see Table 2).

any correspondence with models within  $2\sigma$ . It is important to notice that our sample of galaxies is not complete, so these percentages are just evidence that at least some of these high-redshift ETGs have a less homogeneous stellar population with respect to what is expected in a rigorous passive evolution.

Points that are not consistent with the proposed models at different star formation time-scales cannot be explained by using synthetic models with different *metallicities*. As an example, in Figure 3 the same diagram of Figure 2 is shown, but in this case the different coloured lines represent models with three distinct metallicities ( $Z = 0.008$ ,  $Z = 0.020$  and  $Z = 0.040$ ), at fixed time-scale parameter ( $\tau = 0.1$  Gyr). From Figure 3 it is clear that the not consistent points still remain without a satisfactory explanation on the basis of single-component star formation histories even at different metallicities.

Adding some amounts of dust ( $A_v > 0.5$  mag) in the single component models would marginally help in explaining those data points which have low values of the  $H+K(\text{CaII})$  index (IDs: 1192, 7424 and 9838). However, even this addition is not able to reproduce the index values of four objects with high  $H+K(\text{CaII})$  (IDs: 9066, 10960, 10020 and 1837) because its main effect is to little increase the values of the  $\Delta 4000$  index. Moreover, this choice should be supported by a physical motivation able to justify these quantities of dust in systems where globally the star formation activity should be quenched (age  $\gg \tau$ ).

We have also checked that the values of the two measured indices on synthetic models do not depend on

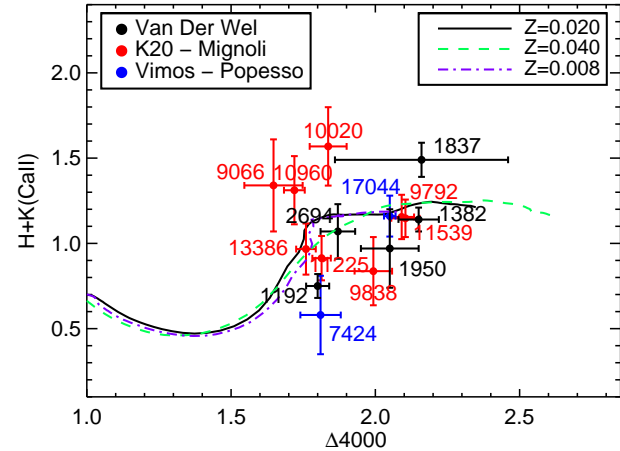


**Figure 3.** Data versus models comparison in the index index plane: measured values of the indices  $\Delta 4000$  ( $x$ -axis) and  $H+K(\text{CaII})$  ( $y$ -axis) from the spectroscopic sample of Van der Wel et al. (2005) (black dots), Mignoli et al. (2005) (red dots) and Popesso et al. (2009) (blue dots), compared with the expectations of BC03 models at different ages (from left to right, from about  $10^8$  to  $10^{10}$  yr), fixed star formation time-scale parameter  $\tau$  and for different *metallicities*:  $Z = 0.008$ ,  $Z = 0.020$  and  $Z = 0.040$  (coloured lines). As in Figure 2, with the exception of those from Van der Wel et al. (2005) sample, shown data points have  $H+K(\text{CaII})$  index values a bit underestimated (within error bars) with respect to those indicated by models due to the difference between the spectral resolutions of BC03 synthetic spectra ( $\text{FWHM} = 3\text{\AA}$ ) and that of the observed ones (see Table 2).

the spectrophotometric models adopted in the analysis: comparing index values obtained from BC03 models with those obtained with the latest version of the same code (Charlot & Bruzual, in preparation), we do not find any difference, while the comparison with Maraston & Stromback (2011) models reveals small differences but well within the observational errors.

The comparison between the measured indices and models has thus suggested that the star formation histories of these galaxies must have been more complex, eventually involving the presence of later star formation events superimposed on a rather old bulk of stars, causing a less homogeneous population than predicted by simple short  $\tau$  models.

A further confirmation of this evidence comes from the discrepancy we found among ages derived from the values of the two indices and those extracted from the SED fitting analysis, as shown in Table 4: the  $\Delta 4000$  index points towards generally more evolved stellar populations. Ages deduced from the index values and reported in Table 4 have been derived assuming BC03 models, solar metallicity and  $\tau = 0.1$  Gyr. Ages deriving from indices and from SED fitting are two different but complementary tools to study the stellar content of galaxies: the spectroscopic analysis is based on a small portion of the SED but it is able to give important details on their recent star formation history, while the photometric analysis can provide mean stellar parameters dealing with the whole SED. This first result thus suggests

**Table 4.** Age estimates derived from indices and photometric analysis (Gyr) obtained from the comparison with synthetic stellar populations models with  $\tau = 0.1$  Gyr and solar metallicity.

ID-MUSIC	Age from H+K(CaII) (Gyr)	Age from $\Delta 4000$ (Gyr)	Age from photometry (Gyr)
1192	1 $\pm$ 0.1	1.9 $\pm$ 0.5	0.7
1382	4.5 $\pm$ 1.5	5.5 $\pm$ 1.5	1.4
1950	1.7 $\pm$ 2	4 $\pm$ 1	0.7
1837	-	5.75 $\pm$ 3	0.9
2694	3 $\pm$ 1.2	2.4 $\pm$ 0.4	1.3
9066	-	0.9 $\pm$ 0.4	1.3
11539	4.7 $\pm$ 1.5	4.75 $\pm$ 0.5	1.3
10020	-	2.2 $\pm$ 0.5	1.3
10960	-	1.1 $\pm$ 0.3	1.4
11225	1.2 $\pm$ 0.5	1.9 $\pm$ 0.4	1.4
9792	4.7 $\pm$ 1.5	4.7 $\pm$ 0.9	2.7
13386	1.4 $\pm$ 0.6	1.5 $\pm$ 0.4	0.6
9838	0.9 $\pm$ 0.3	3.1 $\pm$ 0.4	2.3
17044	1.9 $\pm$ 1	3.75 $\pm$ 0.4	2.3
7424	0.7 $\pm$ 0.4	1.9 $\pm$ 0.5	1.4

that in general the SED analysis is missing small pieces of information, revealed instead by the indices.

Moreover, for many objects (8 out of 15) the ages derived from the  $\Delta 4000$  index tend to differ by more than  $1\sigma$  from those derived from the H+K(CaII) index. In particular, in one case they differ by more than  $2\sigma$  (ID-9838). Furthermore, even if possible, it appears unlikely that the age inconsistency arisen from the two indices is due to measurement errors. Indeed, it would mean introducing a kind of systematicity which should always decrease the values of age derived from the H+K(CaII) index and at the same time always increase those derived from the  $\Delta 4000$  index. In fact, ages from the  $\Delta 4000$  index are older than those indicated from H+K(CaII) index (only for one object there is the opposite trend), in agreement with Onodera et al. (2012) who found similar results for passive galaxies at  $z > 1.4$ . Furthermore, in some cases, ID-2694, ID-9066, ID-10020 and ID-10960 as displayed in Table 4, H+K(CaII) values do not find any age correspondence with models, as visible in Figure 2. As discussed in Section 3, due to the nature of the two selected indices, we expect dissimilarity between them if the galaxy stellar content reveals non-homogeneous properties, especially age. For this reason, having found such a discrepancy in most cases, we started a new analysis of the star formation histories of our sample galaxies assuming that a quite recent star-forming event has been superimposed on an otherwise homogeneous and old stellar population.

As a pure exercise, we have performed the analysis based on the assumption of a double age stellar component for all the galaxies of the sample. The real convenience of introducing the second component, as discussed in the following section, is found only for those objects for which the age values derived from the two indices were not in agreement. And this is the case for 9 out of 15 galaxies. For the remaining galaxies, values of  $\tau \geq 0.1$  Gyr are sufficient to explain the inhomogeneity of their stellar content even though with some corrections to the mean ages derived from the SED fitting analysis.

#### 4.1 Double-component analysis

To better reproduce the observed stellar populations properties of our sample galaxies and in particular to reproduce the measured indices, we thus hypothesized the presence of *composite* stellar populations, assuming that after the initial bulk of star formation, additional events have occurred also in the following few Gyr. For the sake of simplicity, we started introducing only *double* stellar components; we cannot exclude that a more refined analysis which involves more than two spectral index measurements on higher quality spectra could eventually find the presence of triple and over stellar populations.

In Figure 4 (left-hand panel), the comparison of the measured indices with those obtained on synthetic double-component models is shown: models represent galaxies for which the bulk of the stellar mass belongs to a population whose age increases from left to right (from about  $10^8$  to  $10^{10}$  yr) in the index index plane, and small mass fractions are taken into account by a younger component with fixed age 0.5 Gyr. Coloured lines represent the increasing intensity of the secondary burst, i.e. the fraction of the younger component, from the right (dark green line) with a fraction of 0.1 per cent to the left (magenta line) with 2.5 per cent. From this plot, it is clear that with only small mass fractions of a superimposed younger population, observed points with low H+K(CaII) index values can be fully explained.

A similar explanation can be possibly advanced also for points with higher H+K(CaII) index values, but with the addition of a further ingredient. Considering the definition of the H+K(CaII) index, as discussed in Section 3, high index values would mean that the ‘‘H’’ absorption line must be very weak with respect to the K(CaII) line. We then hypothesized that the Balmer H $\epsilon$  line blended with the H(CaII) line is in *emission* rather than in absorption. As shown in Figure 5 in BC03 models, for stellar populations younger than  $< 0.2$  Gyr, Balmer H $\epsilon$  emission is dominant over the absorption. So that the presence of a small mass fraction of very young stellar population (i.e., very recent small burst) can be able to fill the depth of the whole H line, thus increasing the value of the H+K(CaII) index. We



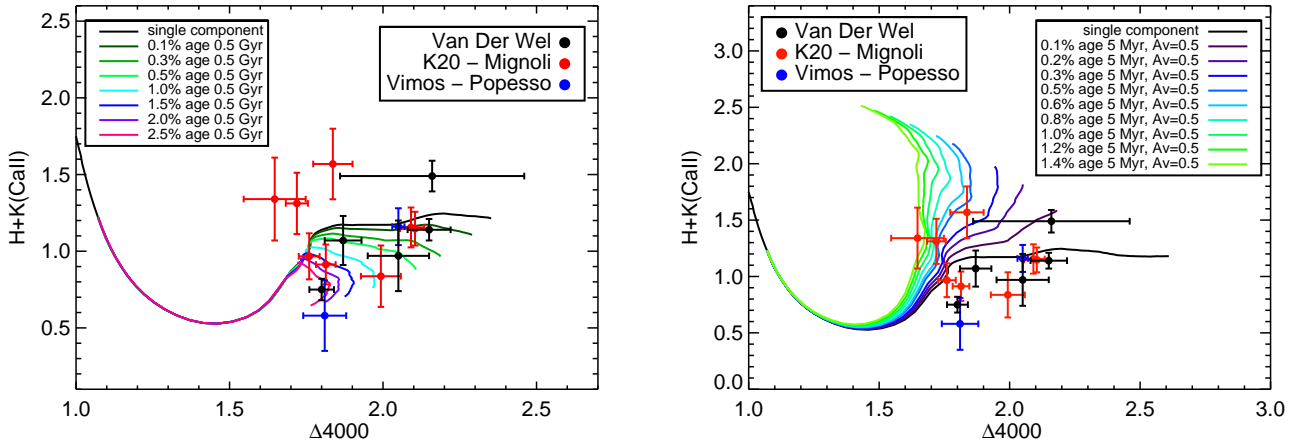


**Figure 4.** Index index plane: comparison with *double-component* models. Left-hand panel: observed points are the same as in Figure 2; lines represent the values of the indices on BC03 synthetic models composed of a main component whose age increases from left to right (from about  $10^8$  to  $10^{10}$  yr), and by small mass fraction of a younger stellar component with age 0.5 Gyr. The fraction of the secondary component increases from 0.1% (dark green line) to 2.5% (magenta line). Right-hand panel: same as the left-hand panel; here the small and younger component has age 5 Myr and it has been reddened with a typical dust extinction of 0.5 mag. Mass fractions span from 0.1% (violet line) to 1.4% (green line). BC03 models are with fixed solar metallicity and  $\tau = 0.1$  Gyr. As in Figure 2 and 3, with the exception of those from Van der Wel et al. (2005) sample, shown data points have H+K(CaII) index values a bit underestimated (within error bars) with respect to those indicated by models due to the difference between the spectral resolutions of BC03 synthetic spectra (FWHM=  $3\text{\AA}$ ) and that of the observed ones (see Table 2). Both plots show how those data points which were not consistent with *single-component* models can be explained.

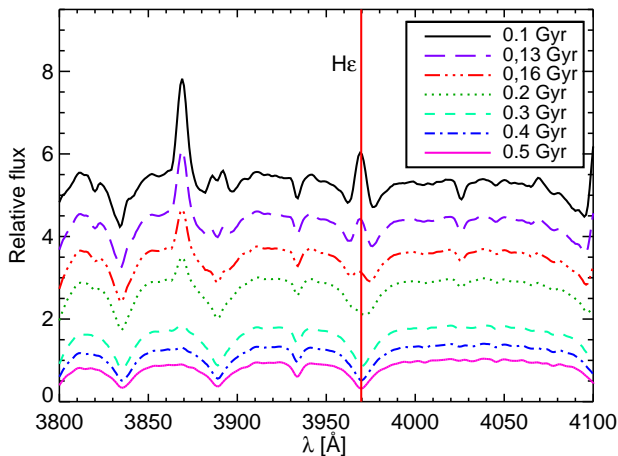


**Figure 5.** Synthetic spectra with Balmer H $\epsilon$  ( $\lambda = 3969.65 \text{\AA}$ , red vertical line) emission line in models at different stellar population ages. Ages decrease from 0.5 Gyr (magenta line) to 0.1 Gyr (black line).

then introduced in our analysis BC03 models which include the nebular emission lines (see Charlot & Longhetti 2001). In fact, as shown in Figure 6, differences between models with emission (cyan solid line) and without emission (black dashed line) are evident for ages smaller than 1 Gyr; for older ages these models coincide. As an example of our analysis, in Figure 4 (right-hand panel) the comparison of model prediction with the observed data in the case of double age component models is shown for a starburst age of 5 Myr. Given the very young age of the secondary component, we

took into account the possible dust extinction that should be acting around it, assuming  $A_v = 0.5$ ; we specify that the introduction of dust affects only the  $\Delta 4000$  index, increasing its value in the same way as age. The intensity of the star formation burst increases from right (violet line), with a mass fraction of 0.1 per cent, to left (green line), with a mass fraction of 1.4 per cent. Both panels of Figure 4 are useful examples that show how the suggested presence of small mass fraction of younger stellar component is able to explain the observed data. Age and percentage of mass involved in the secondary component (i.e., age and strength of the recent burst) can be varied to exactly match each single observation. Below we present the detailed analysis of the whole sample of galaxies and the obtained results.

Each galaxy has been analysed by means of a code that, spanning all the double-component possible models, extracts best-fitting solutions, following the analogue of the one-component photometric analysis. Assuming the BC03 models, including possible emission nebular components, with fixed  $\tau = 0.1$  Gyr and solar metallicity, the code builds all the possible double-component combinations of spectra varying ages, mass fractions and dust extinction of the two stellar components. A maximum age limit has been imposed equal to the age of the Universe at the redshift of each galaxy. Recent burst strengths (i.e. the mass percentage involved in the young component) have been considered by means of 0.05 per cent steps. Dust extinction has been applied both on the whole double-component spectrum and only on the younger component, in parallel distinct analysis, with a 0.1 mag pass.

From the generated composed synthetic spectra our code selects the solutions which are consistent with the measured values of the two spectrophotometric indices within

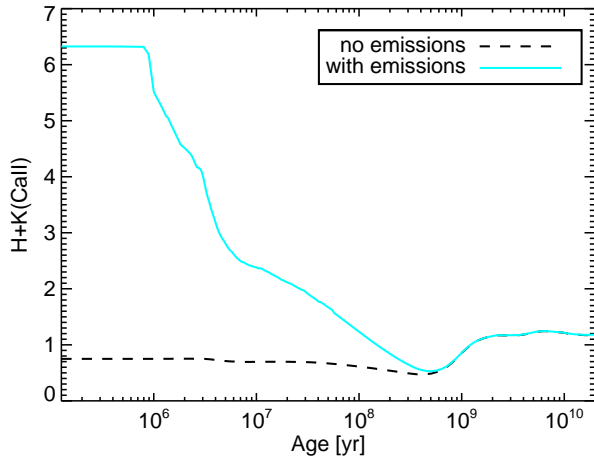


**Figure 6.** Trend of the H+K(CaII) index with age measured on BC03 models with Balmer lines emission (cyan solid line) and without emission (black dashed line). Differences between two models become important only for stellar population with age  $< 1$  Gyr.

their observational errors. After this selection, the code starts the  $\chi^2$  minimization process of the composite synthetic SED on the observed photometric data. In this way not only the optical band is considered, but the whole spectral distribution.

The results of the analysis are shown in Table 6. Mass fraction values expressed in Table 6 are indicative of the amount of mass for the solutions with lower  $\chi^2$  values. The sample objects are well described by two-component models, revealing the consistence of the found solutions with the presence of a younger stellar population for almost all the galaxies of the sample. Moreover, thanks to the procedure applied in our code, all the composite spectra are fully consistent with the measured indices, contrary to the single-component analysis from which this happens only for a couple of objects. Dust extinction in general becomes important, i.e.  $A_v > 2$ , only for objects whose young component is younger than the star formation time-scale parameter  $\tau = 0.1$  Gyr, that means that the star formation is still ongoing.

The improvement in terms of probability  $P(\chi^2)$  of the obtained double-component solutions with respect to the single component ones (with  $\tau = 0.1$  Gyr, see Table 4) is illustrated in Table 5, where we report the comparison of the reduced- $\chi^2$  ( $\chi^2_\nu$ ). The estimation of the  $\chi^2_\nu$  includes both the contribution of the 14 photometric points which constitute the global SED and the values of the two analysed spectral indices. It is worth to remark that in this part of the analysis, for consistency, we have compared the double-component models with the single component ones obtained with fixed small  $\tau = 0.1$  Gyr. Accordingly, the  $\chi^2_\nu$  values and the corresponding probabilities shown in Table 5 are referred to these particular SED fitting solutions.

As can be seen from Table 5, the double-component solutions are preferable over the single component ones for almost all the galaxies of the sample. More in details, for 9 out of 15 galaxies (60 per cent of the sample) (IDs: 1192, 1950, 1837, 9066, 10020, 10960, 9838, 17044 and 7424), which have

the age values derived from indices not in agreement with each other (see Table 4), the double-component solutions with age differences  $> 1.5$  Gyr are clearly more representative of their inhomogeneous stellar contents. For the other six objects, even if providing statistically more probable solutions for four out of six cases, the double-component analysis appears not significantly necessary. Indeed, for these six galaxies the ages derived from the two indices result all in agreement with each other pointing to the same generally older age with respect to the ages extracted from the SED fitting analysis (see Table 4). In particular, for three galaxies (IDs: 1382, 11539 and 9792), the double-component solutions are statistically more probable actually just because the bulk of the mass ( $> 98$  per cent) matches the age indicated by the two indices (compare Table 4 with Table 6), while the single-component solutions miss this important information. Only for the remaining 3 cases (IDs: 2694, 11225 and 13386) both indices and  $\tau \geq 0.1$  Gyr SED fitting analysis point to the same age, directly revealing a rather homogeneous stellar population.

Summarizing, the double-component analysis shows that in 60 per cent of the galaxies of our sample there are two stellar components whose presence explains the different ages derived from the index values. Furthermore, thanks again to the index values, this analysis has confirmed or corrected the ages of the SED fitting solutions for the remaining objects.

In Figure 7, we present two examples of the analysis that we performed on two opposite cases which are not consistent with a single component description: object ID-9066 (top panels) which has a high H+K(CaII) value ( $> 1.2$ ), and object ID-7424 (bottom panels) which has a low value of the H+K(CaII) index. In the caption of Figure 7, we report, as example, the detailed discussion of these two representative cases. Left-hand panels of Figure 7 show the comparison between the single-component (black) and double-component (red) best-fitting solutions on the observed SED (blue points): both the presented double-component models fit better the spectral distributions. Focusing on the  $4000\text{\AA}$  rest frame region (right-hand panels), it can be seen that the double-component spectrum (red) reproduces better the observed spectrum (black) than the single component model (green), in particular the features involved in the H+K(CaII) index definition (i.e. the H and K absorption lines).

#### 4.1.1 The ages of the two stellar components

As we have seen from the analysis of our sample, based on both the spectral indices and the photometric SED fitting, we found evidence that at least 60 per cent of the selected ETGs have the bulk of the mass composed of rather old stars and a small percentage of younger stars. In the following, we include also the three objects (IDs: 1382, 11539 and 9792) for which we have corrected the age of the bulk of stars by means of the index values; indeed, the amounts of younger component, although not necessary, are found to be very small. In this 80 per cent of our sample, which we remark here is not complete, with the exception of object ID-7424, we find that the mass fractions of the younger component are small, less than 10 per cent, with the smallest being 0.05 per cent, while the bulk of the mass belongs to

**Table 5.** Comparison of the reduced- $\chi^2$  and corresponding probabilities between the single and double-component solutions. The  $\chi^2_\nu$  estimations include the comparison among the photometric points and the analysed spectral indices.

ID	$\chi^2_\nu$ single component	Associated probability (%)	$\chi^2_\nu$ double component	Associated probability (%)
1192	5.01	0.7	1.14	32
1382	13.6	0	3.7	16
1950	7.5	0.06	2.94	5
1837	19.94	0	1.31	27
2694	1.56	21	1.8	16
9066	3.31	4	0.66	52
11539	12.66	0	1.16	31
10020	5.02	0.7	0.844	43
10960	3.85	2	1.74	17
11225	0.59	55	0.77	46
9792	9.05	0.01	1.64	19
13386	4.89	0.7	1.16	31
9838	3.43	3	1.26	28
17044	9.87	0.01	1.31	27
7424	2.038	13	1.01	36

**Table 6.** Results obtained from the double-component analysis on the sample of galaxies extracted from the composition of BC03 models, with fixed  $\tau = 0.1$  Gyr and solar metallicity. Mass fractions are the indicative values for the solutions with lower  $\chi^2$  values.

ID	Age young component (Gyr)	Mass fraction (%)	Age old component (Gyr)	Mass fraction (%)	$A_v$ (mag)	Age differences (Gyr)	$z_{form}$ bulk
1192	0.64	6.5	2.4	93.5	0	1.76	2.15
1382	0.1	0.05	5	99.95	0.9 <sup>a</sup>	4.9	6.1
1950	0.45	1	5.5	99	0	5.05	>6
1837	0.015	0.95	5.5	99.05	2.8 <sup>a</sup>	5.485	>6
2694	0.5	0.65	2.3	99.35	0.1	1.8	2.2
9066	0.006	0.75	1.7	99.25	2.8 <sup>a</sup>	1.694	1.95
11539	0.3	0.1	4.75	99.9	0.2 <sup>a</sup>	4.45	>6
10020	0.03	1.5	2.6	98.5	2.3 <sup>a</sup>	2.57	1.45
10960	0.015	1.65	2.3	98.35	2.6 <sup>a</sup>	2.285	1.32
11225	0.9	20	6.25	80	0.2	5.35	>6
9792	0.8	1.65	4.75	98.35	0.3	3.95	2.86
13386	0.1	0.1	1	99.9	0.3	0.9	1
9838	0.5	2.6	4	97.4	0.8 <sup>a</sup>	3.5	2.16
17044	1	5.3	7	96.5	0.2	6	>6
7424	0.7	16.7	6.25	83.3	0.5 <sup>a</sup>	5.55	5.5

<sup>a</sup>  $A_v$  applied only on the young component.

the older component. The distributions of the ages of the old (left-hand panel) and young (right-hand panel) components of this part of the sample, are shown in Figure 8. White data represent the whole 80 per cent of the sample, while blue and green shaded data represent subsamples at respectively  $z \sim 0.7$  and  $z \sim 1$ . Considering the old component age distribution (left-hand panel), it appears bimodal with a younger sample with a mean age of 2.25 Gyr and with an older one of 5.3 Gyr. This means that the bulk of their stars formed at  $1 < z_{form} < 3$  and  $z > 5$ , as it can be seen in Figure 9 which clearly shows that both the two subsamples of galaxies at  $z_{spec} \sim 0.7$  and  $z_{spec} \sim 1$  have a  $z_{form}$  of their main stellar component bimodally distributed, without any dependence on redshift. We remark that this result is evidence coming from a casually selected sample of ETGs and hence it cannot be interpreted as a general bimodality in the distribution of the star formation episodes in ETGs.

On the contrary, in the young component histogram (Figure 8, right-hand panel), the distribution is homogeneous with a mean age of 0.4 Gyr. From both histograms, it is clear that there is no dependence on redshift in the obtained results, so we cannot identify a single confined cosmic period for the formation of the stars neither of the old nor of the younger components.

It is worthy to note that the ages of the bulk components are generally older than the ages derived from the photometric analysis. Indeed, the main components generally reveal the same stellar ages predicted from the values of the  $\Delta 4000$  index, which, as already discussed, is a measure of the global stellar population (see Table 6 in comparison with Table 4). In Figure 10 we report the comparison between the ages estimated from the SED analysis (with fixed  $\tau = 0.1$  Gyr) with respect to both those of the young components (light blue squares) and those of the old components

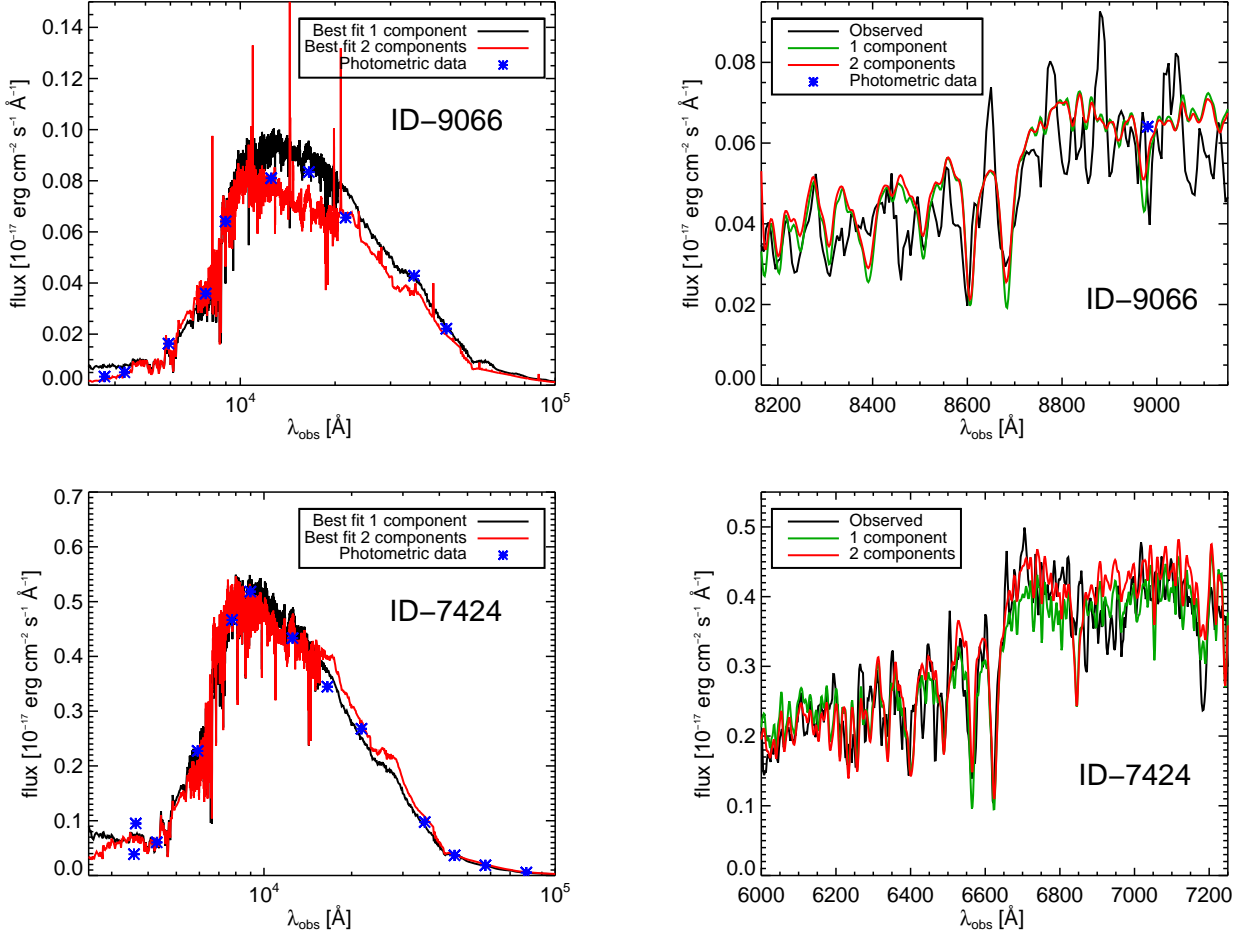


**Figure 7.** Left-hand panels: comparison between single-component solutions (red line) and double-component models (black line) on the observed SED (blue points). Right-hand panels: comparison between single-component spectrum (green) and double-component spectrum (red) on the observed spectrum (black) in the region of the 4000Å rest frame. Upper panels: galaxy ID-9066. Analysis: the corresponding stellar age of this object from the SED fitting analysis was 2 Gyr (with  $\tau = 0.3$  Gyr and  $A_v = 0.6$ , see Table 1); instead, from the index measurements we obtained an age estimate of about 0.9 Gyr from the  $\Delta 4000$  index and none from the H+K(CaII) index because its value is above the critical value (i.e. 1.2). We thus proceeded with the double-component analysis on models with gas emission lines. The result is a composite stellar population with a 6 Myr younger component (with signs of recent star formation) reddened with  $A_v = 2.8$ , superimposed on the bulk of the stellar mass ( $> 99.3$  per cent) with an older age of 1.7 Gyr. The value of the older component age is similar to the photometric age, but the single-component solution was not consistent with the measured indices. Instead the double-component solution, with the adding of small amounts of very young stellar population has been able to adjust the fit of the spectral features, and taking into account at the same time the trend of the whole SED. Bottom panels: galaxy ID-7424. Analysis: from the SED fitting analysis this object was described by a 2.6 Gyr old stellar population with  $\tau = 0.4$  Gyr and  $A_v = 0.2$ , on the other hand, H+K(CaII) and  $\Delta 4000$  indices pointed to ages of 0.7 and 1.9 Gyr respectively (see Table 4). Moreover, the single-component solution was not consistent with the measure of the H+K(CaII) index. The double-component analysis found a consistent solution composed by a main component with old age 6.25 Gyr and a relative high fraction (about 15 per cent) of a young component with age 0.7 Gyr, reddened with  $A_v = 0.5$ .

(dark blue triangles). It can be seen that ages derived from the SED analysis are all younger than 2.7 Gyr, while in our double-component analysis, the ages of the old components reach 7 Gyr. This figure demonstrates that the photometric analysis, without the constraints imposed by the spectrophotometric indices, clearly underestimates the age of the bulk of stars in ETGs at  $z \sim 1$ . As a consequence, it results that also the stellar mass derived from the SED fitting is on average underestimated with respect to the value that can be derived from the double-component analysis. Indeed, we estimate that the mean correction factor for the stellar mass

of our sample galaxies is on average 1.2 with peaks up to a factor of 2, and the more is the difference between the age extracted from the SED fitting and the age of the older component, the higher is the value of this correction.

In conclusion, our results suggest that the bulk of the star formation in our sample ETGs at  $z \sim 1$  happened in two indicative cosmic periods: one at  $z_{form} > 5$  and the other more recent at  $1 < z_{form} < 3$ . New and minor events of star formation occurred in these galaxies within 1 Gyr (upper limit) from their observation, i.e.  $z \sim 1$  and  $z \sim 0.7$ . Again, we point out that these results come from a limited sample

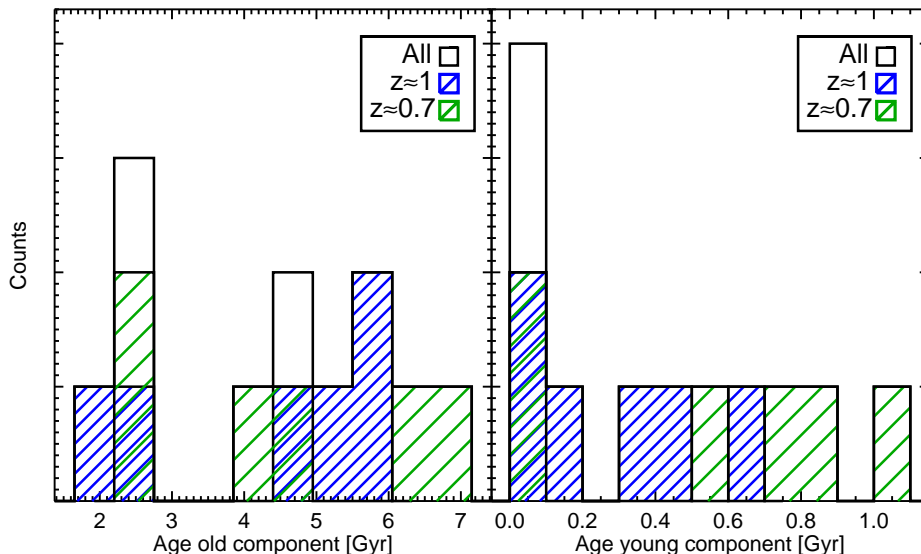


**Figure 8.** Histograms of the double-component analysis results on the 80 per cent of the sample (see Section 4.1.1). White: data from all the 80 per cent of the sample; blue shaded: data from the subsample of galaxies at  $z \sim 0.7$ ; green shaded: data from the subsample of galaxies at  $z \sim 1$ . Left-hand panel: distribution of the ages of the old components in bins of 0.55 Gyr. There are two visible subsets with mean age of about 2.25 Gyr and 5.3 Gyr. Right-hand panel: distribution of the ages of the young components in bins of 0.1 Gyr. The mean age is about 0.4 Gyr.

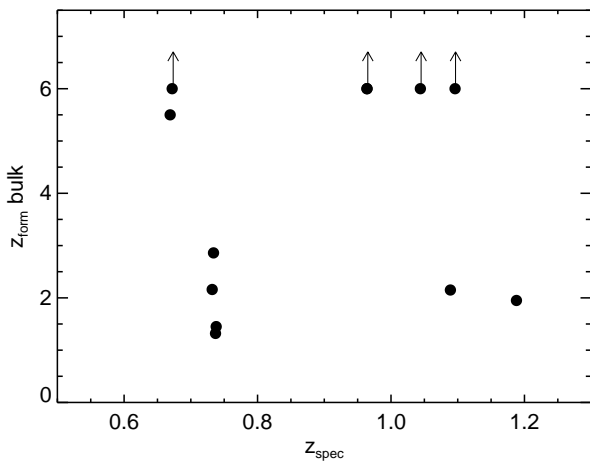


**Figure 9.**  $z_{form}$  of the main component as a function of the  $z_{spec}$  of the 80 per cent of the sample of galaxies. Arrows mean that the values can be higher than what indicated by the respective points.

without any statistics and completeness in  $z$ , so they should be consolidated by means of analysis on larger samples.

It is worthy to note that the obtained results are strictly related to the peculiarities of the two spectrophotometric measured indices. In particular, the H+K(CaII) index has been of fundamental importance to detect the presence of small fractions of young stellar populations also when the bulk of the mass ( $> 98 - 99$  per cent) belonged to the older main component. Indeed, as it appears evident from Figure 4, the H+K(CaII) index experiences large variations even

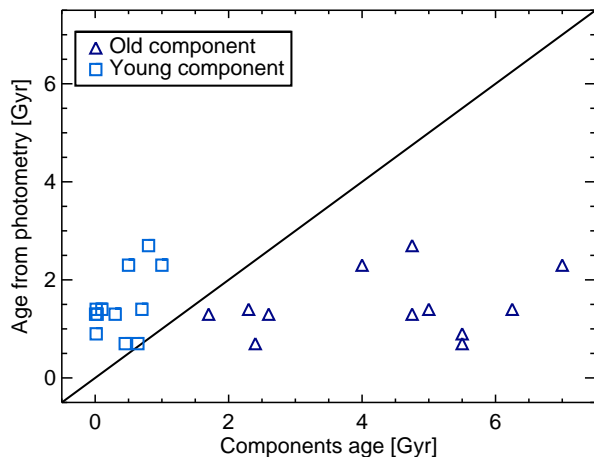


**Figure 10.** Comparison between the ages derived from the SED fitting photometric analysis (from Table 4) and the ages of the main component (dark blue triangles) and the young component (light blue squares) extracted from the double-component analysis (from Table 6). Data concern the 80 per cent of the sample.

when only a small percentage of stellar mass younger than 1 Gyr is added to the old bulk of stars.

## 5 DISCUSSION

In the last years, only two works based on high-redshift ETG optical spectra reported a similar spectroscopic analysis based on spectrophotometric indices. In the following,

**Table 7.** Values of the  $D_n4000$  and  $H\delta_F$  indices (used in Onodera et al. 2012) and  $H\delta_A$  index (used in Jørgensen & Chiboucas 2013) measured on our sample spectra.

ID-MUSIC	$z$	$D_n4000$	$H\delta_F$	$H\delta_A$
1192	1.089	1.59±0.03	2.44±0.53	4.88±0.19
1382	0.964	2.10±0.06	2.15±0.30	0.21±0.60
1950	1.044	1.53±0.08	2.16±0.85	0.48±0.23
1837	0.964	2.28±0.04	1.54±0.34	-1.85±0.24
2694	1.135	1.96±0.07	1.57±0.79	1.13±0.53
9066	1.188	1.71±0.15	4.12±0.62	2.78±3.19
11539	1.096	1.91±0.06	0.05±1.18	-0.70±1.20
10020	0.738	1.78±0.09	1.90±1.25	-0.14±1.95
10960	0.737	1.72±0.05	0.15±0.56	-1.49±0.83
11225	0.736	1.64±0.04	2.06±0.75	1.29±1.13
9792	0.734	1.87±0.05	0.94±0.69	-0.85±1.01
13386	0.734	1.61±0.04	1.58±0.85	0.05±1.30
9838	0.732	1.80±0.08	1.54±1.42	-0.90±2.20
17044	0.672	1.93±0.03	1.09±0.38	1.70±0.54
7424	0.669	1.75±0.09	0.62±1.52	1.20±2.15

we try to compare our results with the finding of these two works.

The first one is a work by Onodera et al. (2012) where the authors present a spectral analysis of a sample of 18 passive elliptical galaxies at  $1.4 < z < 1.8$  in the *Cosmological Evolution Survey* field. In particular, based on near-IR *Subaru/Multi-Object Infrared Camera and Spectrograph* spectra (resolution  $R \simeq 500$ ), they performed the measurements of two spectrophotometric indices in the same region of our analysis: the  $H\delta$  index (defined as  $H\delta_F$  by Worthey & Ottaviani 1997) and  $D_n4000$ , a 4000Å break index definition by Balogh et al. (1999), not coincident with the one adopted in our present work.

To compare our sample with that of Onodera et al. (2012), we have measured the values of the  $H\delta_F$  and  $D_n4000$  indices on the spectra of our sample. Results are listed in Table 7.

In their Figure 17, Onodera and collaborators showed the comparison of their measurements with the predictions of synthetic models (Charlot & Bruzual, in preparation) assuming four different star formation histories and most of their objects are not consistent with any of the displayed models. We add our lower redshift sample in the same  $H\delta_F$  versus  $D_n4000$  plane, and the result is shown in Figure 11 (top panels). Indeed, on average, at fixed  $D_n4000$  index value, the  $H\delta_F$  index value is either higher than expected from models or too low to find any correspondence with models (with  $\tau = 0.1$  Gyr and solar metallicity, black line in Figure 11, top panels). We then proceeded with the same arguments followed in the previous sections, considering double stellar components models. The top-left panel of Figure 11 presents composite models with the younger component at fixed age 0.7 Gyr, while in the top-right panel the minor component is so young, 5 Myr, to present emission lines and to produce negative values of the  $H\delta_F$  index. Double-component models with the adding of gas emission are successful in explaining many of the data points of both samples, in particular those with lower values of both indices. Unfortunately, those points with extreme high values of  $H\delta_F$  (and relative high values of  $D_n4000$  index) remain

still unexplained with any combinations of stellar component ages, as already noticed by Onodera et al. (2012).

Focusing only on our sample data (red points in Figure 11, top panels), it is worth to stress that the obtained spread in the  $H\delta_F$  versus  $D_n4000$  index plane is more restrained than that in the  $H+K(CaII)$  versus  $\Delta 4000$  index plane discussed in this work (see Figure 2). This is due to the lower sensitivity of the  $H\delta_F$  index respect to that of the  $H+K(CaII)$  index to the presence of very small amounts of young stars. As explained in Section 3, indeed, the measure of the H line depth and its ratio with the K line is influenced almost only by the blended  $H\epsilon$  line depth, making the values of their ratio (i.e.  $H+K(CaII)$  index) a very sensible tools for detecting young stellar populations. The larger effectiveness of the  $H+K(CaII)$  index with respect to the  $H\delta_F$  index in finding the younger component is easily verified looking at the synthetic models. Colored lines in Figure 11 (top left panel) indicate the values of the  $H\delta_F$  and  $D_n4000$  indices of double-component models with increasing fractions of the younger component, and it can be noticed that the detachment from the single-component model (black line) is limited with respect to what obtained in Figure 4 in the case of  $H+K(CaII)$  index.

Interestingly, from both top panels of Figure 11, it can be noticed that data points of our sample (red points) stay closer to models than those of Onodera et al. (2012). Since our points refer to lower  $z$  galaxies, we thus looked for a correlation of this spreading with redshift. We separated the entire sample of galaxies in five subsets with different range of redshift:  $z \sim 0.7$ ,  $\sim 1$ ,  $\sim 1.4$ ,  $\sim 1.6$  and  $\sim 1.8$ . In Figure 12, we present the same plot of Figure 11, but with only a representative single-component model (black line, with  $\tau = 0.1$  Gyr and solar metallicity). Colours of the data points go from yellow, low-redshift objects ( $z \sim 0.7$ ), to dark red, the highest redshift ( $z \sim 1.8$ ). From this plot, it is clear that low- $z$  data stay closer to the model than those with high  $z$  and that the more the redshift increases, the more the data are widespread in the index plane, i.e. more distant from models. Furthermore, in Figure 17 in Onodera et al. (2012), the authors present the comparison of their high- $z$  data with local SDSS passive galaxies, and the trend seems to be confirmed: local objects are generally well represented by single-component models with respect to high- $z$  data. In high-redshift objects, differences of ages among possible multiple stellar components are easier to be detected thanks to the younger mean ages, for which even small age differences produce strong signatures (e.g. Balmer lines depth), while in the local Universe the same age differences are almost impossible to be detected for the stellar population ageing, thus vanishing the opportunity of observing the presence of double components. Indeed, two stellar populations with 8 and 12 Gyr, respectively, have almost the same Balmer lines depth. This strengthens the advantage of dealing with direct spectral measurements of higher redshift ETGs in order to study their star formation history.

The second interesting comparison is with the work by Jørgensen & Chiboucas (2013). Their analysis is based on high-S/N optical spectroscopy of the early-type members of three galaxy clusters at  $z > 0.5$  in the framework of the “The Gemini/HST Galaxy Cluster Project” (Jørgensen et al. 2005). We limited our comparison to the highest  $z$  clusters which are the RXJ0152.7-1357 at  $z = 0.83$



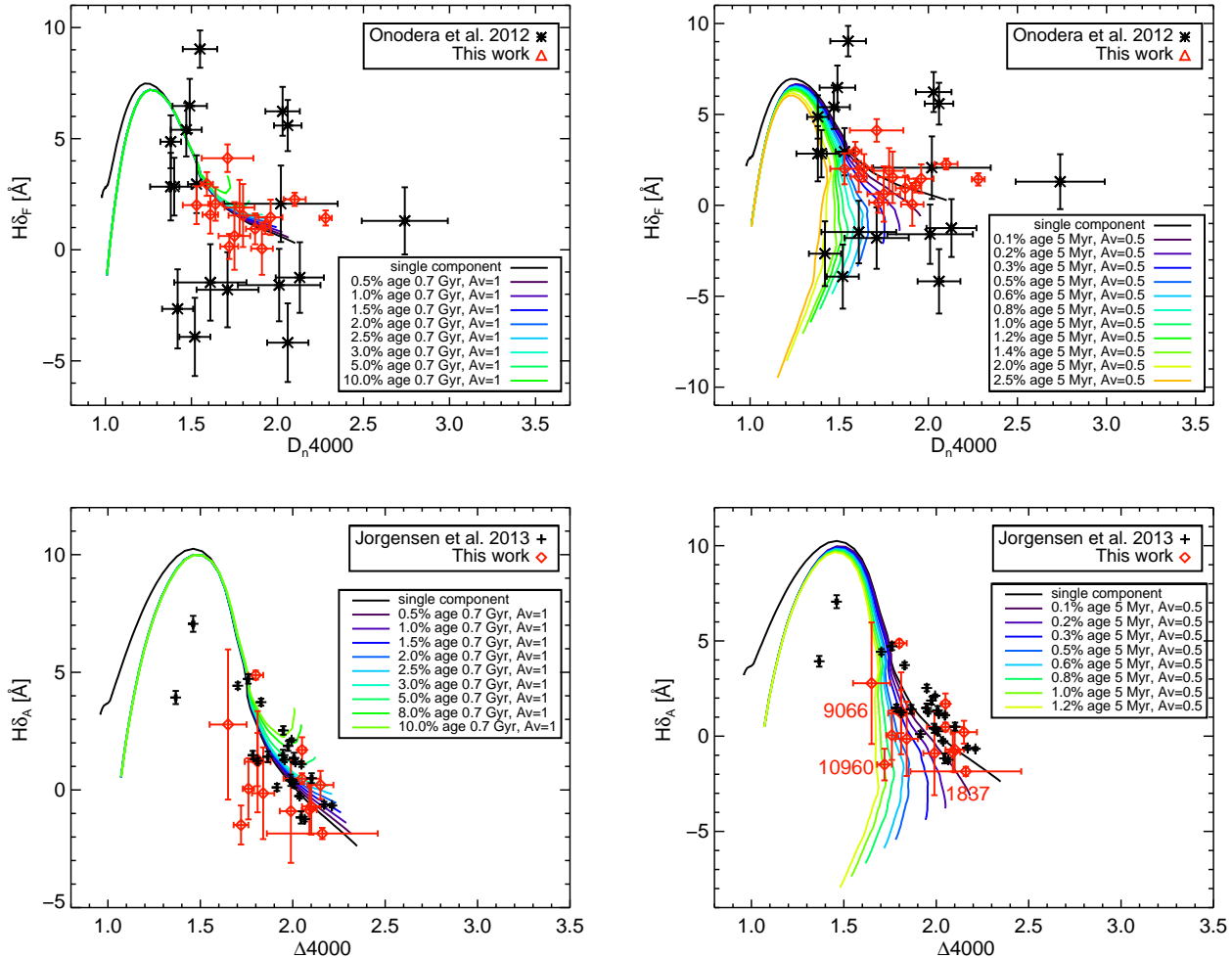


**Figure 11.** Same plots as Figure 4 in the  $H\delta_F$  versus  $D_n4000$  plane, for both the Onodera et al. (2012) sample (black points) and this work sample (red points) (top panels), and in the  $H\delta_A$  versus  $\Delta 4000$  plane for both the Jørgensen & Chiboucas (2013) sample (black points) and this work sample (red points) (bottom panels). Double-component models (coloured lines) are composed of the bulk of the mass whose ages increase from left to right (from about  $10^8$  to  $10^{10}$  yr), and by increasing mass fractions of young component with age 0.7 Gyr with  $A_v = 1$  (left-hand panels), and with age 5 Myr, reddened with  $A_v = 0.5$  (right-hand panels). Double-component models in the right-hand panels are shown with the adding of gas emission lines. In all panels,  $H\delta_F$  values of synthetic models (coloured lines) and data points have been properly corrected to take care of their different spectral resolutions.

and RXJ1226.9+3332 at  $z = 0.89$ , because they match the average redshift of our sample. For these galaxy clusters, in particular, the authors make available the measurements of some spectrophotometric indices obtained from the GMOS-N instrument ( $R = 1918$ ). They adopt the same definition of the  $\Delta 4000$  index as we adopted, and the definition of the  $H\delta_A$  by Worthey & Ottaviani (1997), different from that of Onodera et al. (2012). In order to perform the comparison, we thus measured the values of the  $H\delta_A$  of our sample galaxies, and the results are listed in column 5 of Table 7.

Once again we compared the results with the expectation of the single-component BC03 models (black line, with  $\tau = 0.1$  Gyr and solar metallicity), in Figure 11, bottom panels. Data points from Jørgensen & Chiboucas (2013) (black points) remain relative close to the single-component model predictions (black line), in agreement with the measure of our sample, supporting the previous finding that the secondary younger component is more evident at increasing  $z$ .

In order to preserve the graphic clearness, in Figure 11 only data points belonging to RXJ1226.9+3332 galaxy cluster are shown. In Figure 11, bottom-left panel, we report the comparison of both the two sample data with the double-component models (colored lines), the same as in the top-left panel: points with higher values of  $H\delta_A$  index at fixed  $\Delta 4000$  index value result fully explained by adding a small mass fraction of young stars. On the other hand, only some of our sample data points (red points) have lower values of  $H\delta_A$  index at fixed  $\Delta 4000$  index and they can be again explained with double-component models adding very young stellar components displaying Balmer emission lines. In particular, it is interesting to note that the three objects ID-9066, ID-10960 and ID-1837 of our sample, highlighted with labels in Figure 11 (bottom-right panel), have  $H\delta_A$  and  $\Delta 4000$  indices which are consistent with double-component models displaying emission lines in agreement with the results found using

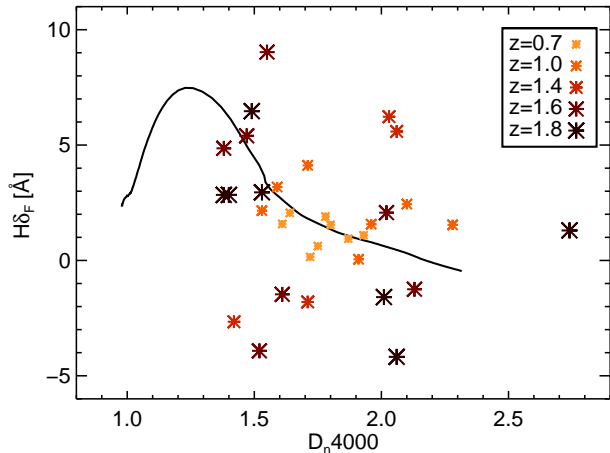


**Figure 12.**  $H\delta_F$  versus  $D_n4000$  plot. Black line is the single-component model with  $\tau = 0.1$  Gyr and solar metallicity. Data from the sample of Onodera et al. (2012) and this work galaxies. Data points are divided into five redshift bins (from yellow to dark red crosses):  $z \sim 0.7$ ,  $\sim 1$ ,  $\sim 1.4$ ,  $\sim 1.6$  and  $\sim 1.8$ . Errors bars are omitted for simplicity; they would be the same as in Figure 11.

the  $H+K(\text{CaII})$  index with respect to the  $H\delta_A$  one in this work (see Figure 4, right-hand panel).

Finally, we remark that in the bottom panels of Figure 11, we are comparing in the same plots data coming from two samples of galaxies at about the same mean redshift but in different environments: our sample (red points) is composed of field galaxies, i.e. low-density environment (with mean  $z = 0.83$ ), while Jørgensen & Chiboucas (2013) sample (black points) is composed exclusively of galaxies belonging to the cluster RXJ1226.9+3332 at  $z = 0.89$ . The fact that the galaxies of the sample of Jørgensen & Chiboucas (2013) do not need on average the presence of a second stellar component modelled with Balmer emission lines, means that in general their stellar populations are homogeneous, i.e. formed in a single or very short burst with no secondary bursts, in agreement with the well-known results of Thomas et al. (2005), where high-density environment galaxies are expected to form their star earlier than low-density counterparts and in a shorter time-scale (see Figure 10 in Thomas et al. 2005). Supposedly, many cluster objects have experienced the same mechanism of star formation and assembling of our sample ETGs that led to the presence of stellar components with different properties, but these events must have occurred earlier in the cosmic time and are less appreciable at the observation redshift.

## 6 SUMMARY AND CONCLUSIONS

We presented a spectroscopic analysis based on the measurements of age-dependent spectrophotometric indices in the region of  $4000\text{\AA}$  rest frame on high-redshift ETGs. We based our analysis on all the up-to-now publicly available optical spectra of ETGs at  $z \sim 1$  in the GOODS-South field, with ascertained morphological classification (see Tamburri et al., in preparation), and with sufficient high-S/N ratio in the region of  $4000\text{\AA}$  break rest frame to allow a detailed spectral

analysis. The sample was then composed of 15 ETGs at  $0.7 < z < 1.1$ , whose spectral data came from three observing campaigns performed by Van der Wel et al. (2005), Mignoli et al. (2005) and Popesso et al. (2009).

From the reduced monodimensional spectra, we have measured the values of the two age-dependent spectrophotometric indices:  $H+K(\text{CaII})$  and  $\Delta 4000$ . The choice of these indices was supported by their sensitivity to the presence of multiple stellar populations with different age. In particular, we have stressed the peculiarity of the  $H+K(\text{CaII})$  index of being very sensitive to age variations even in the case of small amounts of very young stellar content.

From the comparison of the index values with the expectations of single-component BC03 models, we found that many measured values deviate significantly from models. Nor synthetic models with different star formation time-scale  $\tau$  neither those with different metallicity could explain the discrepancy from the ages indicated by the  $\Delta 4000$  index (in general older) and those pointed out by the  $H+K(\text{CaII})$  index. Furthermore, particularly intriguing it was the finding of some values of the  $H+K(\text{CaII})$  index which were too high to find any correspondence with models.

Such a behaviour has thus been attributed to inhomogeneous properties of the stellar populations in the sample galaxies, in particular to age variations. Simple models where the bulk of the star formation happened in a dominant initial event (within a time-scale  $\tau$ ) are not able to explain our results: a further degree of complexity is necessary to understand the star formation history of our sample galaxies. To take into account these inhomogeneities, we then introduced in the modelling a second star formation event, thus considering the stellar population composed of two stellar components which differ from their ages. Adopting composite models, the result is that a small mass percentage of younger stellar component is enough to explain those index values that were not consistent with single-component models. In particular, those high values of the  $H+K(\text{CaII})$  index could be explained introducing the contribution of gas emission lines, due to the presence of star forming regions. Indeed, small mass fractions of very young components ( $< 0.1$  Gyr), where the star formation is still ongoing and the  $\text{H}\epsilon$  Balmer line is in emission, are able to fill the whole H line involved in the  $H+K(\text{CaII})$  index, thus increasing its expected value. From the fitting analysis we obtained that for at least 60 per cent of the galaxies of our sample there are pieces of evidence of the presence of small mass fractions of a younger population coexisting with a much older stellar bulk.

Data suggest that the ages of the *older* components follow two distinct distributions with mean ages of 2.25 and 5.3 Gyr without any correlation with  $z$ , which correspond to mean formation redshift for the bulk of stars at  $1 < z_{\text{form}} < 3$  and  $z_{\text{form}} > 5$ . However, due to the limited number of galaxies of our sample (15) not uniformly distributed in redshift, these results could be only a selection effect. Moreover, we found that the main component ages tend to be older than what concluded from the standard SED fitting analysis (in agreement with Fan et al. 2014 analysis on star-forming galaxies), with some implications on the stellar mass estimate, which results to be underestimated by a factor of  $\sim 1.2$  on average. The following star-forming events (i.e. the *younger* components) are detected



at any redshift of the galaxies of our sample ( $0.7 < z < 1.1$ ), so it cannot be outlined in a common cosmic period in which the younger component has been accreted. It appears more likely that the star formation is triggered steadily over the cosmic time within field ETGs.

We have supposed the presence of younger components also in higher  $z$  sample of passive elliptical (Onodera et al. 2012) up to  $z = 1.8$ , and in  $z \sim 1$  cluster galaxies (Jørgensen & Chiboucas 2013) even if based on the  $H\delta$  index rather than the  $H+K(CaII)$  index, the former less sensible to small amounts of young stellar content. We have found that in general, the ages of the minor younger component are less young for galaxies belonging to cluster, and more extreme with the increasing of redshift.

Having revealed the presence of small young stellar components in many galaxies in a wide redshift range ( $0.7 < z < 1.8$ , thanks to the enlarged sample) implies that there must be a common mechanism by which ETGs at any cosmic time either accrete new amounts of young stellar mass by means of minor merging events, or activate new events of star formation almost constantly over time. Minor merger-induced star formation is the most widely accredited hypothesis to explain the presence of ongoing star formation in ETGs, since it has been also found in the local Universe (Kaviraj et al. 2012). Minor mergers are those with mass ratio ( $M/m$ ) in the range  $1/10 < M/m < 1/4$ , and our findings on the younger components mass fractions are consistent with this scenario. Indeed, adopting the assumption of “dry” minor merging, which in general involves a maximum value of gas fraction of 10 per cent of the total accreted mass (stars+gas), the very small fractions of the second components observed in this work, i.e.  $\sim 0.1$  per cent, result in agreement with this description. On the other hand, obviously, also wet minor merging events are able to explain the origin of the observed younger component, with the accretion of external gas being the driver of new star formation activity. However, minor merging events do not seem to be so frequent in the cosmic epoch from  $z \sim 1$  to now. Indeed, Lopez-Sanjuan et al. (2012) have found that from  $z \sim 1$  to  $z \sim 0$  the number of minor merging per red galaxy is  $0.46 \pm 0.06$ ; thus, it seems rather unlikely that in an albeit small sample of 15 galaxies, we found that at least 9 objects (i.e. 60 per cent) have recently experienced a minor merging event. In addition, it must be considered that all these objects have been classified as ETGs and their morphology appear all regular; thus, if merger events have happened in the cosmic histories of these galaxies, they must have taken place at least few Gyr earlier with respect to their observation in order to resettle the elliptical morphology. But this is not in agreement with our findings where the younger component is always observed with age  $< 1$  Gyr.

Moreover, other independent works, such that by Gargiulo et al. (2012), not only have demonstrated the inhomogeneities of stars in ETGs at  $z > 1$ , but they have also localized the younger component in the inner part of the galaxies. This naturally leads to the question of what is the physical mechanism which, after the external mass accretion by means of hypothetical merging events, is able to bring only the younger stars to the centre of galaxies at least in the case of dry merger event.

On the other hand, our finding of a second younger component also in other high- $z$  samples suggests that the

presence of a small percentage of young stars at any epoch which coexist with the passively evolving older stellar bulk of the galaxy could be common in ETGs. In fact, it is known that ETGs contain small fraction of cold molecular gas that could be converted in star formation activity and its presence has been observationally detected in the local Universe (Lees et al. 1991; Crocker et al. 2011; Panuzzo et al. 2011). This minimal gas reservoir, besides having a presumed external origin, could also be due to the stellar mass loss or may be left over from the initial star formation major burst in the earlier epochs. The favoured scenario is that of the cold accretion: it has been shown (Fardal et al. 2001; Keres et al. 2005; Dekel & Birnboim 2006) that a cold gas mode could be responsible for the star formation in the cosmic history of galaxies and that it can be present, with its filamentary nature and in small quantities, also in spheroidal passive systems where the hot gas mode is dominant. In fact, Keres et al. (2005) show that, from  $z \sim 3$  to  $z \sim 0$  hot gas mode dominated galaxies, i.e. passive and massive spheroids, can form new stars thanks to small amounts of cold gas, and the involved mass fractions,  $< 20$  per cent for stellar masses  $\log(M_*) > 10.5$ , are fully consistent with the detected mass fractions of the younger component in our analysis sample. In addition, this scenario could be in agreement with the observed inner position of the younger component, as the cold gas stream is assumed to infall towards the centre of galaxy attracted by the main potential well.

Thus, the detected young stellar component in the sample of ETGs analysed in the present work suggests that a star formation activity took place steadily over time during the secular evolution of these galaxies, activated by small gas quantities since  $z > 1$ .

## ACKNOWLEDGEMENTS

We thank the anonymous referee of this paper for providing constructive comments that improved the manuscript. This work has received financial support from PRIN-INAF (1.05.09.01.05).

## REFERENCES

- Balogh M. L., Morris S. L., Yee H. K. C., Carlberg R. G., Ellingson E., 1999, ApJ, 527, 54
- Bruzual G., 1983, AJ, 273, 105
- Bruzual G., and Charlot S., 2003, MNRAS, 344, 1000 (BC03)
- Calzetti D., Armus L., Bohlin R.C., Kinney A.L., Koornneef J., and Storchi-Bergmann T., 2000, ApJ, 533, 682
- Cappellari M., et al., 2009, ApJ, 704, L34
- Chabrier G., 2003, PASP, 115, 763
- Charlot S., and Longhetti M., 2001, MNRAS, 323, 887
- Cimatti A., et al., 2004, Nature, 430, 184
- Coccatto L., Gerhard O., and Arnaboldi M., 2010, MNRAS, 407, L26
- Crocker A.F., Bureau M., Young L.M., and Combes F., 2011, MNRAS, 410, 1197
- Daddi E., et al., 2005, ApJ, 626, 680
- Dekel A., and Birnboim Y., 2006, MNRAS, 368, 2

- Fan L., Lapi A., Bressan A., Nonino M., De Zotti G., and Danese L., 2014, RAA, 14, 15
- Fardal M.A., Kats N., Gardner J.P., Hernquist L., Weinberg D.H., and Dave' R., 2001, ApJ, 562, 605
- Gargiulo A., Saracco P., Longhetti M., La Barbera F., and Tamburri S., 2012, MNRAS, 425, 2698
- Glazebrook K., et al., 2004, Nature, 430, 181
- Guo Y., et al., 2011, ApJ, 735, 18
- Hamilton D., 1985, AJ, 297
- Huang S., Ho L.C., Peng C.Y., Li Z., and Barth A.J., 2013, ApJ, 766, 47
- Jørgensen I., Bergmann M., Davies R., Barr J., Takamiya M., and Crampton D., 2005, AJ, 129, 1249
- Jørgensen I., and Chiboucas K., 2013, AJ, 145, 77
- Kaviraj S., et al., 2012, MNRAS, 423, 49
- Keres D., Kats N., Weinberg D.H., and Dave' R., 2005, MNRAS, 363, 2
- Lees J.F., Knapp G.R., Rupen M.P. and Phillips T.G., 1991, ApJ, 379, 177
- Longhetti M., Bressan A., Chiosi C., and Rampazzo R., 1999, A&A, 345, 419
- Longhetti M., and Saracco P., 2009, MNRAS, 394, 774
- Lopez-Sanjuan C., et al., 2012, A&A, 548, A7
- Maraston C., and Stromback, G., 2011, MNRAS, 418, 2785
- Mignoli M. et al., 2005, A&A, 437, 883
- Naab T., Johansson P.H., and Ostriker J.P., 2009, ApJ, 699, L178
- Onodera M., et al., 2012, ApJ, 755, 26
- Oser L., Ostriker J.P., Naab T., Johansson P.H., and Burkert A., 2010, ApJ, 725, 2312
- Oser L., Ostriker J.P., Naab T., and Johansson P.H., 2012, ApJ, 744, 630
- Panuzzo P., Rampazzo R., Bressan A., Vega O., Annibali F., Buson L.M., Clemens M.S., and Zeilinger W.W., 2011, A&A, 528, A28
- Popesso P., et al., 2009, A&A, 494, 443
- Renzini A., ARA&A, 44, 141
- Rocca-Volmerange B., et al., 2013, MNRAS, 429, 2780
- Rose J.A., 1985, AJ, 90
- Sanchez H.D., et al., 2011, MNRAS, 417, 900
- Santini P., et al. 2009, A&A, 504, 751
- Saracco P., Longhetti M., and Gargiulo A., 2010, MNRAS, 408, L21
- Strazzullo V., et al., 2013, ApJ, 772, 118
- Thomas D., Maraston C., Bender R., and de Oliveira C.M., 2005, ApJ, 621, 673
- Treu T., Stiavelli M., Casertano S., Møller P., and Bertin G., 2002, ApJ, 564, L13
- Van der Wel A., Franx M., van Dokkum P.G., Rix H.-W., Illingworth G.D. and Rosati P., 2005, ApJ, 631, 162
- Vanzella E., et al., 2005, A&A, 434, 53
- Vanzella E., et al., 2008, A&A, 478, 83
- Worthey G., and Ottaviani D., 1997, ApJS, 111, 377